Vasopressin lowers renal epoxyeicosatrienoic acid levels by activating soluble epoxide hydrolase

Boldt, C. and Roeschel, T. and Himmerkus, N. and Plain, A. and Bleich, M. and Labes, R. and Blum, M. and Krause, H. and Magheli, A. and Giesecke, T. and Mutig, K. and Rothe, M. and Weldon, S.M. and Dragun, D. and Schunck, W.H. and Bachmann, S. and Paliege, A.

American Journal of Physiology Renal Physiology
2016 DEC 01 ; 311(6): F1198-F1210
2016 SEP 28 (first published online)
doi: 10.1152/ajprenal.00062.2016

Publisher: American Physiological Society (U.S.A.)

Articles in PresS. Am J Physiol Renal Physiol (September 28, 2016). doi:10.1152/ajprenal.00062.2016

Vasopressin lowers renal epoxyeicosatrienoic acid levels by activating soluble epoxide hydrolase

C. Boldt[1*], T. Röschel[1*], N. Himmerkus[2], A. Plain[2], M. Bleich[2], R. Labes[1], M. Blum[3], H. Krause[4], A. Magheli[4], T. Giesecke[1], K. Mutig[1], M. Rothe[5], S.M. Weldon[6], D. Dragun[7,8], W.H. Schunck[3], S. Bachmann[1], and A. Paliege[7,8]

*contributed equally

Department of Anatomy, Charité-Universitätsmedizin Berlin, Berlin, Germany[1]
Department of Physiology, Kiel, Germany[2]
Max Delbrueck Center for Molecular Medicine, Berlin, Germany[3]
Department of Urology, Charité-Universitätsmedizin Berlin, Berlin, Germany[4]
Lipidomix GmbH, Berlin, Germany[5]
Boehringer Ingelheim Pharmaceuticals Inc., Ridgefield, Connecticut, USA[6]
Department of Nephrology, Charité-Universitätsmedizin Berlin, Berlin, Germany[7]
Berlin Institute of Health (BIH), Berlin, Germany[8]

Running title: Vasopressin activates renal soluble epoxide hydrolase

Address correspondence to: Alexander Paliege, MD (alexander.paliege@charite.de) or Sebastian Bachmann (sbachm@charite.de), Philippstr. 12, D-10115, Berlin, Germany. Fax: +49 30 - 450 528 922

ABSTRACT

Activation of the thick ascending limb (TAL) Na^+-K^+-$2Cl^-$-cotransporter (NKCC2) by the antidiuretic hormone arginine-vasopressin (AVP) is an essential mechanism of renal urine concentration and contributes to extracellular fluid and electrolyte homeostasis. AVP effects in the kidney are modulated by locally and/or by systemically produced epoxyeicosatrienoic acid derivates (EET). The relation between AVP and EET metabolism has not been determined. Here we show that chronic treatment of AVP-deficient Brattleboro rats with the AVP V2 receptor analog desmopressin (dDAVP; 5ng/h, 3d) significantly lowered renal EET levels (-56 ± 3% for 5,6-EET, -50 ± 3.4% for 11,12-EET, and -60 ± 3.7% for 14,15-EET). The abundance of the principal EET-degrading enzyme soluble epoxide hydrolase (sEH) was increased at the mRNA (+160 ± 37%) and protein levels (+120 ± 26%). Immunohistochemistry revealed dDAVP-mediated induction of sEH in connecting tubules and cortical and medullary collecting ducts, suggesting a role of these segments in the regulation of local interstitial EET signals. Incubation of murine kidney cell suspensions with 1 µM 14,15-EET for 30 min reduced phosphorylation of NKCC2 at the AVP-sensitive threonine residues T96 and T101 (-66 ± 5%; $p<0.05$) while 14,15-DHET had no effect. Concomitantly, isolated perfused cTAL pretreated with 14,15–EET showed a 30% lower transport current

under high and a 70% lower transport current under low symetric chloride concentrations. In sum, we have shown that activation of AVP signaling stimulates renal sEH biosynthesis and enzyme activity. The resulting reduction of EET tissue levels may be instrumental for increased NKCC2 transport activity during AVP-induced antidiuresis.

KEYWORDS

urine concentration mechanism, thick ascending limb, NKCC2

INTRODUCTION

Water conservation by the mammalian kidney is achieved by the tightly controlled, coordinate action of epithelial and vascular components. The hypothalamic antidiuretic hormone (arginine-vasopressin, AVP) plays a dominant role herein. It stimulates luminal insertion of water channels along the connecting tubule and collecting duct epithelia, and of urea transporters into medullary portion of the collecting duct **(37)**. The thick ascending limb (TAL) is sensitive to AVP as well, since abundance, phosphorylation, and surface expression of the furosemide sensitive Na^+-K^+-$2Cl^-$-cotransporter (NKCC2) are stimulated by the hormone **(37)**. At the vascular level, AVP causes vasoconstriction of preglomerular arterioles and descending vasa recta and thereby reduces medullary blood flow. The combination of an augmented solute transport activity and a reduced perfusion facilitates efficient countercurrent multiplication but also results in a marked hypoxia of key medullary structures **(17)** which may promote the development of renal disease **(5)**. The renal effects of AVP are modulated by locally produced arachidonic acid derivates such as 20-hydroxyeicosatetraenoic acid (20-HETE), epoxyeicosatrienoic acids (EET), and prostaglandin E2 (PGE2) which inhibit TAL transport activity **(1, 15, 26, 31, 57)** and increase medullary perfusion **(4, 74)**. While the regulation of 20-HETE and PGE2 during AVP-induced antidiuresis has been studied in considerable detail **(59, 73, 77),** less is known regarding the mechanisms which determine synthesis and metabolism of EET in this setting. EET exist as four regioisomers, 5,6-EET, 8,9-EET, 11,12-EET, and 14,15-EET which are synthesized by the cytochrome p450 (CYP450) monooxygenases **(18, 57)**. CYP450 isoforms 2C9/10, 2C11, 2C23, 2J3, and 2J4 have all been shown to contribute to renal EET synthesis (18, 19, 34). In rats, 2C23 is considered the principal renal isoform to generate EET in rat kidney (34). EET are metabolically degraded mainly by soluble epoxide hydrolase (sEH) which hydrolyses EET to their corresponding, less active dihydroxyeicosatrienoic acid isomers (DHET) **(31, 57)**. The preferred substrates for sEH are 14,15-EET, 11,12-EET, and 8,9-EET whereas the affinity of the enzyme towards 5,6-EET is low **(30)**. The kidney shows substantial sEH activity, but the site of its synthesis and regulation within the renal parenchyma has not been univocally clarified **(19, 33, 38, 48, 75)**. Earlier, microarray-based gene expression studies have provided evidence for AVP-dependent activation of sEH in the kidney **(17, 51),** prompting us to study the effects of AVP on renal medullary EET metabolism in greater detail.

In the present study, we found that sEH is abundantly expressed in the segments of human and rat nephrons and collecting duct system. Chronic AVP treatment induced sEH biosynthesis in AVP-deficient Brattleboro rats, which was associated with a reduction of renal EET levels. Functional studies in isolated

TAL segments demonstrated an inhibitory effect of 14,15-EET on NKCC2 phosphorylation and transport activity. Induction of sEH by AVP may therefore be an essential mechanism for the maintenance of sustained antidiuresis.

MATERIALS AND METHODS

Animal studies and tissue preservation. Animal studies were performed according to NIH guidelines after approval by the Berlin council on animal care (permission numbers G006-02/05, G0285/10, and O0124/96). For localization studies adult Sprague Dawley (SD) rats (n = 3) were perfusion-fixed via the abdominal aorta using a fixative containing 3% paraformaldehyde (Merck, Darmstadt, Germany) dissolved in PBS as previously described **(52)**. Kidneys were harvested and processed for cryostat and paraffin sectioning using established methodology **(51)**. For Western blot analysis of zonal sEH distribution additional SD rats (n = 3) were killed by cervical dislocation. Kidneys were carefully removed and dissected into cortex, outer medulla and inner medulla using sterile razor blades and a stereotactic microscope. Samples were subsequently snap frozen in liquid nitrogen, and stored at -80°C until further use. Human kidney samples (n = 3) were obtained from the healthy parts of tumor nephrectomy specimen after written consent of the patients. Tissue blocks were immersion-fixed for 12 h using 3% paraformaldehyde in PBS and subsequently processed for paraffin embedding (46). Detailed protocols for treatment of Brattleboro rats with 1-desamino-8-D-Arg vasopressin (dDAVP) have been published before **(51)**. Briefly, Brattleboro rats aged 2-3 month (n = 26) were treated with normal saline as vehicle or dDAVP (n = 13 each; 5 ng/h for 3 days; Sigma Aldrich, Munich, Germany) via subcutaneous infusion using osmotic minipumps (ALZET osmotic minipump model 2001, Charles River, Sulzfeld, Germany). At the end of the treatment period animals for microarray (n = 3 per group) and biochemical studies (n = 5 per group) were sacrificed by cervical dislocation. Kidneys were carefully removed and processed at 4 °C. Samples were snap frozen in liquid nitrogen, and stored at -80 °C until further use. Animals for morphological studies (n = 5 per group) were perfusion fixed as detailed above. sEH deficient mice were originally obtained from Boehringer Ingelheim Pharmaceutical Inc. (Ridgefieldt, CT, USA) and bred in the animal facility of the Max Delbrück Center for Molecular Medicine in Berlin. A detailed description for the establishment of gene deletion and genotyping has been published **(41, 62)**. Animals were backcrossed into FVB/N background for at least 6 generations **(28)**. At three month of age kidneys of male knockout and wild type mice (n = 4 for each genotype) were harvested for biochemical analysis or fixed overnight using 3% paraformaldehyde in PBS and processed for histological studies. Microdissection of murine TAL segments was performed as previously described **(9)** using a total of 6 male C57/Bl6 mice (Charles River, Sulzfeld, Germany).

Microarray studies. Gene expression profiling studies were conducted in the microarray facility at the Zentrum für Medizinische Forschung of the University Mannheim (Mannheim, Germany) as previously described **(17, 51)**. Affymetrix rat genome 230 2.0 arrays and a custom CDF version 9 annotation with Unigene based gene definitions

(http://brainarray.mbni.med.umich.edu/Brainarray/Database/CustomCDF/CDF_download_v9.asp) were used for the analysis. Raw and normalized data were deposited in the Gene Expression Omnibus database (http://www.ncbi.nlm.nih.gov/geo/; GEO accession number: GSE34225).

Quantification of renal outer medullary lipid levels. Free tissue lipid levels were determined by mass spectrometry in kidney samples of dDAVP treated Brattleboro rats and controls. Samples were powdered in liquid nitrogen, dissolved in a 50/50 v/v mixture of water/and methanol supplemented with 0,01% butylhydroxytoluol, mixed with 10 µL internal standard solution (0,5 µg/mL), andbuffered at pH 6 with 2 mL SPE-buffer (0.1 mol/L aqueous sodium acetat solution, pH 6). Solid-Phase-Extraction was performed using a Bond-Elut-Certify-II-Column (Phenomenex, Torrance, USA). Eicosanoids were eluted with 2 ml n-hexan/ethylacetat (25/75 v/v) with 1% acetic acid. The solvent was evaporated with a gentle stream of N_2 at 40°C. Residues were resuspended in 100 µL methanol/water mixture and processed for measureing. Liquid chromatography-mass spectrometry (LC-MS/MS) was performed at the mass spectrometry facility of Lipidomix GmbH as previously described (Lipidomix GmbH, Berlin, Germany) **(2)**. Free tissue levels of EET isomers and of the linoleic acid epoxides 9,10-EPOME and 12,13-EPOME and their respective diols 9,10-DIHOME and 12,13-DIHOME were determined in parallel. Since the formation of these diols is also catalyzed by sEH the ratio of DIHOME and EPOME isomers can be utilized as measure for sEH tissue activity **(20, 68)**.

Real time polymerase chain reaction (PCR). mRNA was isolated from whole kidney homogenates using Roti-Aqua phenol-chloroform extraction kit according to the manufacturer's protocol (Carl Roth, Karlsruhe, Germany). After digestion of genomic DNA by DNAse 1 treatment (Qiagen, Hilden, Germany) cDNA was generated by reverse transcription using the Applied Biosystems cDNA synthesis kit (Applied Biosystems, Darmstadt, Germany). TaqMan quantitative RT-PCR for sEH was performed using the Applied Biosystems probe Mm00514706 and the 7500 Fast Real-Time PCR system (Applied Biosystems) following the manufacturer's instructions. The mRNA levels of GAPDH were determined in parallel and served as loading control (catalogue number 4352338E, Applied Biosystems). Expression levels were calculated using the $2^{-\Delta\Delta CT}$ method and expressed as % of control **(40)**.

Primary antibodies. For detection of sEH we used an affinity purified rabbit antibody against human sEH (1:500, HPA023094, Atlas Antibodies, Stockholm, Sweden). Antibodies against total and phospho-(p)-T96/T101-NKCC2 were generated in our laboratory and have been described before (46). Antibodies for cyclooxygenase 2 (COX-2; sc-1746) and aquaporin 2 (AQP2; sc-9882) were obtained from Santa Cruz Biotechnology (Dallas, Texas, USA). Antibody against the Na^+-Cl^--cotransporter NCC was provided by D. Ellison (OHSU, Portland, USA) and served as a marker for the distal convoluted tubule **(51)**. Antibody for the proximal tubule marker megalin was a kind gift of T. Willnow (MDC, Berlin, Germany) and has been described before **(3)**. Antibody against mouse alpha-smooth muscle actin was from DAKO (Hamburg, Germany); antibody for β-actin was from Sigma-Aldrich.

Immunoblotting. Samples for Western blotting were prepared as previously described **(71)**. Briefly, tissues were ground in liquid nitrogen using sterile mortar and pestle and subsequently dissolved in homogenization buffer containing 250 mM sucrose, 10 mM triethanolamine, and protease inhibitors (cOmplete protease inhibitor cocktail, Roche Diagnostics, Indianapolis, USA). Nuclei were removed by centrifugation (1000 x g for 10 min). Protein concentration of post nuclear homogenates was determined using bicinchoninic acid protein assay following the manufacturer`s instructions (Thermo Fisher Scientific, Bonn, Germany). Samples were subsequently separated by SDS polyacrylamide gel electrophoresis in a 10% gel (50 µg protein/lane) and electrophoretically transferred to nitrocellulose membranes. Primary antibodies were applied after blocking of nonspecific protein binding sites with 5% non-fat dry milk in PBS. Membranes were incubated for 1 h at room temperature followed by an overnight-incubation at 4° C. Bound antibody was detected using the appropriate HRP-conjugated secondary antibodies and chemiluminescence. Developed X-ray films were scanned and densitometrically evaluated using the Alpha Imager software (Cell Biosciences, Santa Clara, USA). Expression levels were normalized to the expression of the housekeeping gene β-actin.

Immunostaining. Immunofluorescence and immunoperoxidase staining were carried out as previously described **(51)**. Briefly, 4 µm paraffin sections were deparaffinized, rehydrated and subjected to antigen retrieval by boiling in 0.1 M sodium citrate buffer using a pressure cooker. Non-specific binding sites were blocked by incubation with 5% dry milk in PBS. Renal localization of sEH was studied by immunofluorescence staining on 4 µm paraffin sections of human and rat kidneys using the rabbit anti sEH antibody in a 1:100 dilution. Immunoreactive nephron segments were characterized by double labeling with the established segment-specific antibodies to NKCC2 (1:5000 dilution) for TAL, COX-2 (1:100 dilution) for macula densa, NCC (1:100 dilution) for distal convoluted tubule, and AQP2 (1:100 dilution) for connecting tubule and collecting duct, respectively. Bound antibodies were detected with the appropriate Alexa488 or Cy3-labeled secondary antibodies (Dianova, Hamburg, Germany). Stained sections were examined by confocal microscopy using a Zeiss LSM Exciter confocal microscope and ZEN 2008 software (Carl Zeiss, Jena, Germany). Sections for immunoperoxidase staining were prepared as detailed above. Tissue peroxidases were blocked with 3% hydrogen peroxide in methanol prior to application of the primary antibodies. Signal was developed using HRP-labelled donkey anti rabbit secondary antibody (Dianova) and 3,3′-diaminobenzidine containing 0.3% hydrogen peroxide (Sigma-Aldrich); samples were processed synchronously with standardized incubation times to ensure comparability of the measurements.

Validation of sEH antibody. Antibody-specificity was verified by immunoblotting in sEH knockout tissue and by peptide blockade in rat kidney sections. To this end we performed Western blot on total kidney homogenates from sEH deficient mice and their respective controls. Peptide blockade studies were conducted using the immunizing peptide (APrEST76223, Atlas antibodies, Stockholm, Sweden). sEH

antibody was diluted in 5% nonfat dry milk in PBS and incubated at 37° C for 30 minutes with different amounts of blocking peptide prior to application to rat kidney sections. Western blotting and immunostainings were performed as described above.

Renal tubule perfusion. Freshly isolated cTAL segments of 10 male C57/Bl6 mice (Charles River, Sulzfeld, Germany)were incubated with either 0.34% ethanol (control) or with 1 µM 14,15-EET (Cayman Chemicals, Ann Arbor, Michigan, USA) in 0.32% ethanol or 1 µM 14,15 -DHET (Cayman Chemicals, Ann Arbor, Michigan, USA) in 0.34% ethanol for 30-40 min at 30° C in incubation solution (140 mmol/l NaCl, 0.4 mmol/l KH_2PO_4, 1.6 mmol/l K_2HPO_4, 1 mmol/l $MgCl_2$, 10 mmol/l Na-acetate, 1 mmol/l α-ketogluterate, 1.3 mmol/l Ca-gluconate, 3.75 mg/ml glycine, 0.48 mg/ml trypsin inhibitor, 0.25 mg/ml DNAse I, and 5 mg/ml albumin, pH7.4). All chemicals were obtained from Merck (Darmstadt, Germany) unless indicated otherwise. Preincubated cTALs were then transferred into the bath on a heated microscope stage. The bath was heated to 37°C and continuous bath perfusion at 3-5 ml/min with control solution (140 mmol/l NaCl, 0.4 mmol/l KH_2PO_4, 1.6 mmol/l K_2HPO_4, 1 mmol/l $MgCl_2$, 5 mmol/l glucose, 1.3 mmol/l Ca-gluconate, pH7.4) was obtained by gravity perfusion. Tubules were held and perfused by a concentric glass pipette system. The perfusion pipette was double-barreled, and barrel one was used for voltage measurement and perfusion (perfusion rate 10-20 nl/min; 7.6 ± 0.3 µm inner diameter) with control solution. Barrel 2 was used for constant current injection (13 nA) and perfusion with low Cl^- solution (28 mmol/l NaCl, 0.4 mmol/l KH_2PO_4, 1.6 mmol/l K_2HPO_4, 1 mmol/l $MgCl_2$, 5 mmol/l glucose, 1.3 mmol/l Ca-gluconate, 51 mmol/l mannitol, 62 mmol/l $NaSO_4$, pH7.4). After an equilibration period under symmetric control conditions, first the basolateral, then the luminal solution was changed to low Cl^-. Cable equations were used to calculate transepithelial resistance R_{te} as described **(21)**. Equivalent short circuit current I'_{sc} was calculated from R_{te} and V_{te} according to Ohms law, for both conditions respectively. The percentage of I'_{sc} under low Cl^- in relation to the I'_{sc} under high Cl^- (V_{max}) was calculated as the measure of Cl- affinity of the transporter (9). The effects of the EET isomers on NKCC2 phosphorylation were determined using mouse kidney cell suspensions. To this end kidneys of adult male C57/Bl6N mice were flushed with incubation solution to remove the blood. Kidneys were subsequently incubated for 10 min in incubation solution containing 1mg/ml collagenase 2 (Sigma-Aldrich) for collagenase digestion. After complete digestion the cells were pelleted by centrifugation at 1000g for 10 min, collagenase solution was discarded and the pellet resuspended in fresh incubation solution containing 100 nM dDAVP to induce NKCC2 phosphorylation. Aliquots of the resulting cell suspension were treated for 30 min at 37°C with 5,6-EET, 8,9-EET, 11,12-EET, 14,15-EET and 14,15-DHET (1µM final concentration; Cayman Chemicals) or with ethanol as vehicle. After the treatment cells were pelleted at 1000g for 10 min and prepared for Western blot analysis as described above.

Statistical analysis. All values are given as means ± SEM. Statistical analysis was performed using unpaired Student's *t*-test or ANOVA with post hoc Tukey´s test. Null hypothesis was excluded when P was < 0.05.

Results

Effect of dDAVP on medullary expression of EET-metabolizing enzymes. Screening of Affymetrix microarray results from kidney extracts of dDAVP or vehicle treated Brattleboro rats revealed constant mRNA levels for the CYP monooxygenases in CYP2C11, CYP2C23, CYP2J3, and Cyp2J10 (Table 1). Abundance of CYP2J4 mRNA was reduced by 20% relative to the vehicle treated controls ($p < .05$) but subsequent real time PCR verification studies in a separate set of animals (n = 5 per group) failed to confirm differential regulation (data not shown). mRNA levels for sEH were significantly induced (+145% relative to controls; $p < 0.05$) and in the real time PCR verification studies (+160 ± 37%, $p < 0.05$).

Effect of dDAVP on renal free EET tissue levels. Mass spectrometry analysis of renal lipid levels in dDAVP-treated Brattleboro rats revealed a reduced abundance of 5,6-EET (12.8 ± 3.2 ng/g vs. 35.7 ± 9.5 ng/g; $p < .05$), 11,12-EET (16.7 ± 3.3 ng/g vs. 38.4 ± 9.7 ng/g; $p < 0.05$), and 14,15-EET (11.2 ± 3 ng/g vs. 34.7 ± 9.2 ng/g; $p < 0.05$) relative to controls. Levels of the 8,9-isomer showed a strong trend towards reduced levels (17.4 ± 4 ng/g vs. 44 ± 13.4 ng/g; $p = 0.08$) but failed to reach the level of statistical significance. Values are given as ng EET/g wet tissue weight in dDAVP and vehicle treated animals with n = 7 to 8 animals per group (Fig. 1). It must be noted that 5,6-EET rapidly forms a lactone in aqueous solutions which may differ from the parent molecule in its biological activity. During the tissue processing for our mass spectrometry assay this lactone is converted back to 5,6-EET. Thus, the measured levels for the 5,6-EET regioisomer may be higher than the biologically active levels in the tissue.

We also determined the levels of the linoleic acid epoxides 9,10-EPOME (69 ± 14 ng/g vs. 254 ± 60 ng/g; $p < 0.05$) and 12,13-EPOME (36 ± 11 ng/g vs. 166 ± 44 ng/g; $p < 0.05$) as well as their respective diols 9,10-DIHOME (52 ± 8.8 ng/g vs. 47 ± 8.7 ng/g; $p = 0.7$ n.s.) and 12,13-DIHOME (85 ± 25 ng/g vs. 56 ± 14 ng/g; $p = 0.4$ n.s.) in dDAVP-treated Brattleboro rats and controls. The ratios for 9,10-DIHOME and 9,10-EPOME (0.85 vs. 0.23; n = 7 to 8 animals per group; $p < 0.05$) and 12,13-DIHOME and 12,13-EPOME (2.54 vs. 0.43; n = 7 to 8 animals per group; $p < 0.01$) were significantly increased in the dDAVP-treated animals thus demonstrating increased sEH enzyme activity (Fig. 2).

Characterization of sEH antibody. Specificity of the sEH antibody was verified by peptide blockade and by immunoblotting on kidney samples of sEH deficient mice. Preincubation of sEH antibody with the immunizing peptide caused a dose-dependent decrease in signal intensity in rat kidney sections. Blockade was maximal at ten-fold excess of the blocking peptide (Fig. 3A). Western blot analysis of kidney homogenates from wild type mice revealed the presence of a dominant sEH-immunoreactive band at 63 kDa which was absent in the homogenates of the sEH deficient mice. An additional band was detected at 70 kDa. However, this band was also present in the sEH-deficient mice and was therefore considered unspecific (Fig. 3B).

Renal distribution of sEH. Zonal distribution of sEH was analyzed on rat kidney homogenates isolated from cortex and outer and inner medulla. Distribution of NKCC2 was determined in parallel and showed abundant signal in the outer medulla, weaker signal in the cortex and absence of signal in the inner medulla thus confirming the adequate separation of the kidney zones. Western blot for sEH revealed a dominant immunoreactive band at approximately 63 kDa which was present in all kidney zones. Samples from the inner medulla contained additional sEH-immunoreactive products at 50 and 48 kDa which probably represent splice variants of the enzyme (Fig. 3C) **(27)**.

Immunofluorescence labeling of rat and human kidney sections confirmed abundant expression of immunoreactive protein in all kidney zones (Figures 3-6). In the cortex strong cytosolic sEH signal was found in profiles of the macula densa as indicated by the coexpression COX-2 (Fig. 4A-C). Coexpression of sEH and COX-2 was further detected in a subset of cells in the cortical TAL (Fig. 4D-F) whereas the remaining TAL was devoid of staining. Principal cells of the connecting tubule and the cortical collecting duct were identified by their expression of AQP2 and showed abundant sEH signal (Fig. 4G-I). Triple labeling with the Na^+-Cl^--cotransporter NCC demonstrated the complete absence of sEH from the distal convoluted tubule (Fig. 4I). Profiles of the proximal tubule displayed subapical signal with intermediate intensity which was localized directly below the megalin immunoreactive brush border membrane (Fig. 4J-L). Signal intensity increased towards the end of the S3 segment and extended into the thin descending limb of the loop of Henle (Fig. 5A-C). Profiles of the thin ascending limb of the loop of Henle stained positive as well (Fig. 5D-F). Strong staining for sEH in the outer medulla was further detected in the collecting ducts which were typically in close proximity with NKCC2 expressing profiles of the thick ascending limb thus suggesting functional interaction (Fig. 5G-I). Staining in the inner medulla was localized to tDLH, tALH, and to the principal cells of the inner medullary collecting duct as indicated by the coexpression of AQP2 (Fig. 5J-L). Since immunohistochemistry does not allow the distinction between the full-length protein and the shorter products, the observed signals in the inner medulla reflect the sum of the full-length protein and the shorter variants.

The renal vasculature, as identified by the expression of alpha smooth muscle actin in myocytes and pericytes of the vascular wall, was devoid of sEH staining (Fig. 6). Studies in human kidney samples confirmed the expression in the macula densa and in the collecting duct using the sEH antibody validated in rodent tissue together with NKCC2 or AQP2 co-staining (Fig. 7).

Effect of chronic dDAVP treatment on renal sEH expression. The effects of a chronic activation of the urine concentrating mechanism on renal sEH expression were studied in dDAVP-treated Brattleboro rats. Functional data for these animals demonstrating augmented urine concentration and induced levels of NKCC2 and aquaporin 2 have been reported before **(17, 51)**. Immnuohistochemistry revealed icreased sEH protein levels in the cortex and in the outer medulla of dDAVP-treated animals. Here sEH signal was strongly increased in connecting tubules and in the cortical and outer medullary collecting ducts. Protein levels in the inner medulla remained unchanged (Fig. 8A). Western blot analysis of total kidney homogenates confirmed increased levels of the 63 kDa (+65 ± 7% compared to controls; $p < 0.05$) and the

50 kDa (+65 ± 7% compared to controls; $p < 0.05$) variant of the protein in the dDAVP treated animals (Figure 8B-C).

Effect of EET regioisomers on TAL transport activity and NKCC2 phosphorylation. The acute effects of the different EET regioisomers on the phosphorylation of NKCC2 were determined in murine kidney cell suspensions pre-stimulated with 100 nM dDAVP. Incubation of these cell suspensions with the individual EET regioisomers resulted in a significant reduction of pNKCC2 abundance for 5,6-EET, 8,9-EET and 14,15-EET when compared to the vehicle-treated controls (-35 ± 14%, -53 ± 8%, and -66 ± 5%, respectively; $p < 0.05$). In contrast, 11,12-EET had no effect (+18 ± 15%, $p = 0.5$) (Fig. 9). To corroborate these results we studied the effects of the 14,15-EET regioisomer in greater detail and also included the inactive metabolite 14,15-DHET. Phosphorylation of NKCC2 functionally changes the transport current by changing NKCC2 membrane trafficking as well as by changing its Cl^- affinity, rate-limiting in the cortical TAL with already dilute luminal fluid (9, 22). To investigate the effect of 14,15-EET on TAL tubular transport we therefore measured the equivalent short circuit current I'_{sc} under two Cl^- concentrations, at 147 mmol/l to as assess maximal transport velocity ("V_{max}") of the transporter and at 30 mmol/l, a concentration close to the described EC50 of NKCC2 for Cl^- (22). Freshly isolated cTAL were incubated with either vehicle (control), 1µmol/l 14,15 –EET or 1 µmol/l 14,15-DHET for 30-40 min. After this preincubation period isolated perfused cTALs of the three groups, Control, 14,15-EET and 14,15-DHET, showed the typical lumen positive transport I'sc. Pretreatment with 14,15-EET reduced I'sc to 70% of the control I'_{sc} under high Cl- concentration and to approx. 30% under the low Cl- concentration, respectively (Fig.10 A). To address the question if 14,15-EET only reduces the total amount of NKCC2 in the plasma membrane, thereby shifting the curve in the scheme (Fig. 10 B) from 1 to 2, or also decreases its Cl-affinity (curve 3 in the scheme) we calculated the percentage of I'sc (low Cl-) of the respective "V_{max}" (147 Cl-) values (Fig. 10 B). 14,15-EET treatment led to a 55% reduction indicating a markedly reduced Cl-affinity. In contrast, pretreatment with 14,15-DHET did not induce a change in any of the parameters. Treatment of murine kidney cell suspensions with100 nM dDAVP and 14,15-EET at concentrations of 0.1 or 1 µM resulted in a dose-dependent reduction of pNKCC2 levels when compared to cell suspensions treated with 100 nM dDAVP and ethanol as vehicle (control). Treatment with 1 µM 14,15-DHET had no effect on the NKCC2 phosphorylation (Fig. 10D).

Effect of sEH gene disruption on NKCC2 phosphorylation. Analysis of outer medullary pNKCC2 abundance revealed greatly reduced levels in the sEH-deficient mice relative to the wild type controls (Figure 11) whereas total NKCC2 abundance was unchanged (data not shown).

DISCUSSION

Aim of the present study was to characterize the effects of AVP on the abundance and metabolism of EET isomers in the kidney. We have demonstrated markedly reduced tissue levels of EET isomers along with

an increased abundance of the principal EET-metabolizing enzyme sEH in connecting tubules and collecting ducts of AVP-treated Brattleboro rat kidneys as compared to vehicle treated controls. EET isomers and AVP have been shown to exert opposing effects on essential renal sodium transporters. In CNT and CD, AVP activated the amiloride-sensitive epithelial sodium channel ENaC **(5, 6),** whereas 14,15-EET acted as potent inhibitor of ENaC transport activity **(13)**. In the TAL, AVP caused activation of NKCC2-dependent ion transport in part by increasing its phosphorylation (46). In the present study we found a pronounced inhibitory effect of all EET regioisomers with the exception of 11,12-EET on NKCC2 phosphorylation. Parallel microperfusion studies on murine cortical TAL segments demonstrated an inhibitory effect of 14,15-EETon the chloride sensitivity of NKCC2 and overall TAL transport activity. In line with this, sEH-deficient mice, which display elevated tissue levels of EETs and 20-HETE **(41, 62)**, showed markedly reduced phosphorylation of NKCC2. These findings agree with data by He et al. on the inhibitory effects of 14,15-EET on NKCC2 transport activity in cultured murine macula densa cells **(26)**. By contrast, Grider et al. found no effect of 10^{-8} M 5,6-EET on transport activity in isolated rat TAL segments **(23)**. However, the 5,6-EET concentration used in that study was well below the free tissue concentrations observed in our study and may therefore have been insufficient to inhibit NKCC2-dependent transport. Opposing effects of AVP and EETs have further been described for the renal vasculature. Here, AVP causes vasoconstriction either directly by activating vascular V1 receptors or indirectly by its effects on epithelial V2 receptors **(8, 45, 67),** whereas EETs may function as vasodilating mediators in afferent arterioles and interlobular arteries (Review in **(30)**). The observed reduction of renal EET levels in response to AVP may therefore be instrumental for sodium retention and increase in renovascular resistance during AVP-mediated urine concentration.

Cellular sources and regulation of renal EET synthesis during antidiuresis have not been clarified satisfactorily in previous work. The first rate-limiting step during the formation of EETs is the release of arachidonic acid from membrane phospholipids which is typically catalyzed by a phospholipase A2 (PLA2) isoenzyme. The identity of the PLA2 isoenzyme involved in the synthesis of EETs has not been elucidated. However, in a previous study we have shown that the calcium-independent isoform of PLA2 (iPLA2β) is abundantly expressed in the connecting tubule and medullary collecting duct, and that chronic stimulation with dDAVP led to a reduction of iPLA2β biosynthesis, with the assumed consequence of reduced AA release **(51)**. Since both, connecting tubule and collecting duct have been identified as important sites for intrarenal EET production **(65)**, reduced iPLA2 levels at these sites may likely have contributed to the reduced abundance of EETs observed in the present study. Alternative pathways for arachidonic acid release have been described but their relevance for renal EET synthesis remains to be determined **(16, 36)**. The next step in the biosynthesis of EETs is catalyzed by a CYP monooxygenase isoenzyme, however, based on the results of microarray studies CYP monooxygenase abundance was not affected by AVP. This finding argues against a relevant role of CYP monooxygenases as rate limiting enzymes in EET metabolism under this condition. Here we have, however, identified an additional mechanism for the regulation of EET levels in response to AVP, which centrally involves the function of sEH.

So far, ample evidence has linked sEH to the pathophysiology of cardiovascular and renal disease, and inhibitors of sEH have been shown to exert antihypertensive and renoprotective effects **(33, 34, 38, 44, 53, 58)**. In spite of extensive studies performed on the renal expression of sEH, however, there is still no consensus regarding the intrarenal localization of the enzyme. Earlier reports range from an exclusively vascular localization **(75)** over interstitial **(53)** to preferentially glomerular **(38)** or tubular expression **(33)**. In our study we found widespread distribution of the protein with expression in proximal tubules, ascending and descending thin limbs of the loop of Henle, the macula densa and in CNT and CD whereas glomeruli, medullary TAL and DCT, and vascular structures were devoid of staining. Little is currently known regarding the function of sEH in individual nephron segments. In the proximal tubule, 5,6-EET and 14,15-EET haves been shown to inhibit sodium transport **(29, 39, 42, 64).**Expression of sEH in the apical membrane of proximal tubules may therefore serve to deactivate EETs in the tubular fluid to avoid uncontrolled inhibition of transport. Another important finding of our study is the abundant expression of sEH in macula densa and cortical TAL and its colocalization with COX-2 at these sites. COX-2-derived prostaglandins cause vasodilation of the afferent arteriole and thereby play an important role for the maintenance of glomerular filtration during impaired renal perfusion **(24)**. However, COX-2 is also capable of oxidizing 5,6-EET, and the resulting metabolites have been shown to cause vasoconstriction of the preglomerular vasculature **(31)**. sEH activity in the macula densa and the cortical TAL may therefore reduce local EET-levels and may thus prevent the formation of vasoconstrictive metabolites. Notably, we found high levels of sEH also in the inner medulla, where we and others had previously detected abundant COX-2 expression **(12, 70, 73)**. Again, sEH may serve to prevent the formation of EET-metabolites with unwanted properties at this site.

The dDAVP-treated Brattleboro rats revealed elevated sEH levels in CNT and CD which corresponds to the established localization of the AVP V2 receptor **(46, 50, 60)** and suggests a functional link between AVP-signaling and sEH activation. Although a mechanism for this link has so far not been explored, the analysis of the sEH promotor sequence revealed the presence of several putative cAMP-response elements in our hands. AVP-dependent induction of sEH biosynthesis may therefore be mediated via the AVP V2 receptor-dependent activation of adenylyl cyclase VI **(56)**. Other mediators which have been shown to regulate sEH biosynthesis and may interfere with AVP signaling include angiotensin II (32, 69, 72, 78), steroid hormones (43, 55) and PPAR gamma agonists (25, 47).

The potential biological relevance of an AVP-dependent activation of sEH is illustrated by observations in several animal models for renal and cardiovascular disease. Along this line, spontaneously hypertensive rats displayed increased renal sEH activity compared to their normotensive Wistar Kyoto counterparts **(76)** along with elevated plasma levels of AVP **(11, 14)** and an increased abundance of renal AVP receptors **(66)**. Hypertension in these animals could be effectively reduced by treatment with antagonists for AVP **(63)** or sEH **(35)**. Parallel protective effects of antagonists for AVP and sEH have also been described for DOCA-salt-induced hypertension **(10, 49, 54)**, systolic heart failure **(44),** or diabetic nephropathy **(7)**. Based on our findings we thus suggest that the detrimental effects of AVP may in part be mediated by its

effect on sEH synthesis and the resulting accelerated degradation of vasodilatory and transport-inhibiting EET.

In summary, we have shown that activation of AVP signaling causes upregulation of renal sEH biosynthesis and enzyme activity. The resulting reduction of EET tissue levels may facilitate increased transport activity and renal vasoconstriction to promote antidiuresis, but it may as well render the kidney susceptible to insult. Further characterization of the AVP-sEH-EET axis may therefore provide new targets for renoprotective therapeutic strategies.

ACKNOWLEDGEMENTS

We thank F. Grams, K. Riskowsky, and C. Andrée for technical assistance and A. Drobbe for editorial support.

GRANTS

These studies were supported by the Deutsche Forschungsgemeinschaft (FOR667 and FOR1368).

DISCLOSURES

No conflicts of interest are declared by the authors.

FIGURE LEGENDS

Table 1. *Microarray analysis of dDAVP effects on outer medullary mRNA levels of soluble epoxide hydrolase and cytochrome p450 monooxygenases.* Analysis of published microarray data of kidney extracts from dDAVP-treated Brattleboro rats shows strong induction of sEH mRNA levels as compared to vehicle-treated controls, whereas the mRNA abundance of the principal cytochrome p450 monooxygenases, Cyp2c11, Cyp2c23, Cyp2j3, and Cyp2j10 are unaltered. Cyp2j4 mRNA shows a modest decrease which, however, could not be reproduced by alternative technology. Data are derived from (51) and presented as x-fold of vehicle-treated controls; * $p < 0.05$; n = 3 per group.

Figure 1. *Effect of dDAVP treatment on outer medullary free EET levels in Brattleboro rats.* Quantification of outer medullary free EET concentrations reveals significantly lower levels of 5,6-EET, 11,12-EET, and 14,15-EET upon 5ng/h dDAVP for 3 days as compared to vehicle treated controls. 8,9-EET reduction failed to be significant ($p = 0.08$). Data are the mean ± SEM; * $p < 0.05$; n = 7 to 8 per group.

Figure 2. *Effect of dDAVP treatment on outer medullary levels of linoleic acid derivates in Brattleboro rats.* Quantification of outer medullary levels of epoxide (EPOME)- and dihydroxy (DIHOME)-derivatives of linoleic acid reveals an increased DIHOME/EPOME ratio; this suggests increased activity of sEH **(61).** * $p < 0.05$; ** $p < 0.01$; n = 7 to 8 per group.

Figure 3. *Verification of anti-sEH antibody and distribution of sEH protein. A)* Representative micrographs documenting labeling of rat kidney sections with rabbit anti sEH antibody (I) or with rabbit anti sEH antibody following preincubation with the immunizing peptide (II). Abundant signal for sEH is present in the macula densa, proximal tubule and collecting duct profiles (I). Preincubation of sEH antibody with the immunizing peptide results in a dose-dependent reduction of immunofluorescence signal. Blockade was maximal at ten-fold excess of the peptide (II). Immunofluorescence staining; bar indicates 20 µm. *B)* Western blot analysis of kidney homogenates of wild type (lanes 1-2) and sEH deficient mice (sEH -/-; lanes 3-4) showing a dominant band at 63 kDa in the wild type animals whereas no product is present in the sEH -/- kidneys, thus confirming the specificity of the antibody. *C)* Western blot analysis of the zonal distribution of sEH reveals a dominant immunoreactive band at approximately 63 kDa which is present in all kidney zones. Samples from the inner medulla contain additional immunoreactive products at approximately 50 and 48 kDa which probably represent splice variants of sEH **(27)**. Western blot for NKCC2 shows abundant signal in the outer medulla, weaker signal in the cortex and absence of signal in the inner medulla thus confirming the adequate separation of the kidney zones. β-actin serves as loading control.

Figure 4. *Localization of sEH protein in Sprague Dawley rat kidney.* Representative micrographs documenting double labeling of rat kidney sections with rabbit anti sEH antibody (A,D,G,J) and Cyclooxygenase 2 (COX-2; B,E) as a marker for the macula densa segment, the Na^+-Cl^--cotransporter NCC as a marker for the distal convoluted tubule (DCT; magenta in I), aquaporin 2 (AQP2) as a marker for the principal cells of the connecting tubule (CNT; H), and megalin as a marker for the proximal tubule (K). In the merged color images (C,F,I,L), red signal indicates sEH, and green signals mark COX-2 (C,F), AQP2 (I), and megalin (L), respectively. Magenta signal in (I) marks NCC. Macula densa (between flanking lines in (C)) shows strong signal for sEH and COX-2 (A-C). sEH and COX-2 are also coexpressed in a subset of TAL cells distant to the juxtaglomerular apparatus (JGA; D-F). Abundant signal for sEH is present in the AQP2 immunoreactive CNT principal cells (G-I). DCT profiles are negative for sEH (G-I). Proximal convoluted tubule shows subapical sEH signal beneath megalin staining (J-L). Immunofluorescence staining; bars 20 µm; blue nuclei (Dapi); (G), glomerulus in C; (*), TAL in F. Dashed line in I marks the transition from DCT (+) to CNT (#).

Figure 5. *Localization of sEH protein in Sprague Dawley rat kidney (continued).* Representative micrographs documenting double labeling of rat kidney sections with rabbit anti sEH antibody (A,D,G,J) and megalin (B) as a marker for the proximal tubule (PT), Na-K-2Cl-cotransporter NKCC2 (E,H) as a marker for the thick ascending limb (TAL), and aquaporin 2 (AQP2; K) as a marker for the medullary collecting duct. In the merged color images (C,F,I,L), red signal indicates sEH, and green signals mark megalin (C), NKCC2 (F,I), and AQP2 (L), respectively. PT sEH signal is localized subapically (A-C). Signal is stronger within terminal S3 and ensuing descending thin limb (DTL) portions (arrows in C) and

continues to ascending thin limb (ATL; + in F) until its transition to the negative TAL (* in F,I). Abundant sEH signal is present in the principal cells of the collecting duct in the outer (G-I) and inner medulla (J-L). Double labeling with NKCC2 shows the close local association between sEH expressing collecting ducts (# in I) and profiles of the TAL in the outer medulla (G-I). In the inner medulla sEH is abundantly expressed in DTL, ATL and collecting ducts, with partial overlap to AQP2 in the latter (J-L). Immunofluorescence staining; bars 20 μm; blue nuclei (Dapi). The dashed line in F marks the transition from ATL to TAL.

Figure 6. *Localization of sEH protein in the renal vaculature.* Representative micrographs documenting double labeling of rat kidney sections with rabbit anti sEH antibody (A,D,G,J) and alpha smooth muscle actin (B,E,H,K; α-sma) as a marker for the vascular wall. In the merged color images (C,F,I,L), red signal indicates sEH and green signals mark α-sma. There is complete separation of the two signals, demonstrating absence of sEH from vascular smooth muscle and endothelial cells of afferent arterioles (A-C), arcuate vessels (D-F) and vasa recta of outer (G-I) and inner medulla (J-L). Immunofluorescence staining; bars 20 μm; blue nuclei (Dapi); (G), glomerulus, and (*), afferent arteriole in C; (+), lumen of an arcuate vein, and (§), lumen of an arcuate artery in F.

Figure 7. *Localization of sEH protein in the human kidney.* Double labeling of human kidney sections with rabbit anti sEH antibody (A,D,G) and antibodies against NKCC2 (B,E) or aquaporin 2 (AQP2; H). In the merged color images (C,F,I), red signal indicates sEH, and green signals mark NKCC2 (C,F) and AQP2 (I). Ample sEH protein is expressed in the macula densa (between flanking lines in (C) whereas the cells of the surrounding TAL are negative. Strong staining is also present in outer and inner medullary collecting duct profiles. Immunofluorescence staining; bars 20 μm; (G), glomerulus in C; (*), TAL in F; #, collecting ducts in F and I.

Figure 8. *Effect of chronic vasopressin V2 receptor activation on sEH protein expression in Brattleboro rats. A*) Representative high power micrographs showing sEH signal in the cortex (I,II), outer medulla (III,IV) and inner medulla of Brattleboro rats after vehicle (I,III,V; control) or dDAVP treatment (II,IV,VI; dDAVP). Treated animals show a stronger accumulation of immunoreactive sEH in the cortex and outer medulla compared to controls. Inner medullary sEH signals are not different. Immunoperoxidase staining; bars 100 μm; n = 8 per group. *B)* Western blot of kidney homogenates from Brattleboro rats treated with vehicle or dDAVP showing increased signal intensity for the 63 and 50 kDa sEH variants ; β-actin served as loading control. *C)* Densitometric analysis of the signal confirms increased total abundance of sEH in the treated animals. Data are means ± SEM; * $p < 0.05$; n = 8 per group.

Figure 9. *Effect of EET regioisomers on NKCC2 phosphorylation. A)* Western blots of murine kidney cell suspensions treated with 100 nM dDAVP as control (-) or with 100 nM dDAVP and 1 μM 5,6-EET, 8,9-EET, 11,12-EET or 14,15-EET (+) for 30 min. Bands show lower levels of phosphorylated NKCC2

(pNKCC2) after treatment with 5,6-EET, 8,9-EET and 14,15-EET; total NKCC2 abundance was determined in parallel and serves as loading control. *B)* Densitometric analysis of the signal intensity and normalization to total NKCC2 levels confirms reduced abundance of pNKCC2 after treatment with 5,6-EET, 8,9-EET, and 14,15-EET. No effect is detectable following treatment with 11,12-EET. Data are means ± SEM; ** $p < 0.01$; n = 8-10 per group. Samples were prepared from a total of 6 mice.

Figure 10. *Effects of 14,15-EET on TAL transport activity and NKCC2 phosphorylation. A)* Summarized data of the equivalent short-circuit current I'sc of isolated perfused cTAL pretreated with vehicle (control; empty bars), 1 µM 14,15-EET (black bars) or 1 µM 14,15–DHET (grey bars) under two symmetric Cl- concentrations, 30 mmol/l Cl- (30) and 147 mmol/l Cl- (147). *B)* Simplified scheme to illustrate enzyme kinetic like properties of NKCC2 (curve 1) with maximal transport rate (V_{max}, dashed line). Reduced number of NKCC2 in the membrane reduces V_{max} with unchanged EC 50 (curve 2). Changes in Cl- affinity of NKCC2 lead to an additional shift of EC 50 to higher Cl^- concentrations (curve 3).
C) I'_{sc} at low chloride concentration expressed as percentage of the respective V_{max} values; the 55% reduction after 14,15–EET pretreatment shows a markedly reduced Cl^- affinity. Treatment with 14,15-DHET has no detectable effect on $I'_{sc.}$ Ectrophysiological data are means ± SEM, n=8,9,8; * $P < 0.05$ control vs. 14,15–EET; # $P < 0.05$ 14,15-EET vs.14,15–DHET. *D)* Western blot of dDAVP-stimulated murine kidney cell suspensions showing a dose-dependent reduction of phosphorylated NKCC2 (pNKCC2) after treatment with 0.1 µM and 1 µM 14,15-EET as compared to the vehicle treated control. Treatment of dDAVP-stimulated kidney cell suspensions with 14,15-DHET has no effect. Total NKCC2 abundance was determined in parallel and serves as loading control. Representative example of n = 9 for vehicle-, EET-, and DHET, respectively. Samples were prepared from a total of 6 mice.

Figure 11. *Effect of sEH deficiency on outer medullary levels of phosphorylated NKCC2 (pNKCC2).* Representative low (I,II) and high (III,IV) power micrographs showing reduced levels of immunoreactive pNKCC2 in the outer medulla of sEH deficient mice (II,IV; sEH -/-) compared to wild type controls (I,II). Immunoperoxidase staining; bars 200 µm for I, II, and 20 µm for III, IV. n = 4 per group.

References

1. **Amlal H, Legoff C, Vernimmen C, Paillard M, and Bichara M**. Na(+)-K+(NH4+)-2Cl- cotransport in medullary thick ascending limb: control by PKA, PKC, and 20-HETE. *The American journal of physiology* 271: C455-463, 1996.
2. **Arnold C, Markovic M, Blossey K, Wallukat G, Fischer R, Dechend R, Konkel A, von Schacky C, Luft FC, Muller DN, Rothe M, and Schunck WH**. Arachidonic acid-metabolizing cytochrome P450 enzymes are targets of {omega}-3 fatty acids. *The Journal of biological chemistry* 285: 32720-32733, 2010.
3. **Bachmann S, Schlichting U, Geist B, Mutig K, Petsch T, Bacic D, Wagner CA, Kaissling B, Biber J, Murer H, and Willnow TE**. Kidney-specific inactivation of the megalin gene impairs trafficking of renal inorganic sodium phosphate cotransporter (NaPi-IIa). *Journal of the American Society of Nephrology : JASN* 15: 892-900, 2004.

4. **Badzynska B, and Sadowski J**. Opposed effects of prostaglandin E2 on perfusion of rat renal cortex and medulla: interactions with the renin-angiotensin system. *Exp Physiol* 93: 1292-1302, 2008.
5. **Bankir L, Bouby N, and Ritz E**. Vasopressin: a novel target for the prevention and retardation of kidney disease? *Nat Rev Nephrol* 9: 223-239, 2013.
6. **Bankir L, Fernandes S, Bardoux P, Bouby N, and Bichet DG**. Vasopressin-V2 receptor stimulation reduces sodium excretion in healthy humans. *Journal of the American Society of Nephrology : JASN* 16: 1920-1928, 2005.
7. **Bankir L, Roussel R, and Bouby N**. Protein- and diabetes-induced glomerular hyperfiltration: role of glucagon, vasopressin, and urea. *American journal of physiology Renal physiology* 309: F2-F23, 2015.
8. **Boertien WE, Meijer E, de Jong PE, Bakker SJ, Czerwiec FS, Struck J, Oberdhan D, Shoaf SE, Krasa HB, and Gansevoort RT**. Short-term renal hemodynamic effects of tolvaptan in subjects with autosomal dominant polycystic kidney disease at various stages of chronic kidney disease. *Kidney international* 84: 1278-1286, 2013.
9. **Borschewski A, Himmerkus N, Boldt C, Blankenstein KI, McCormick JA, Lazelle R, Willnow TE, Jankowski V, Plain A, Bleich M, Ellison DH, Bachmann S, and Mutig K**. Calcineurin and Sorting-Related Receptor with A-Type Repeats Interact to Regulate the Renal Na+-K+-2Cl- Cotransporter. *Journal of the American Society of Nephrology : JASN* 27: 107-119, 2016.
10. **Brooks VL, Freeman KL, and Qi Y**. Time course of synergistic interaction between DOCA and salt on blood pressure: roles of vasopressin and hepatic osmoreceptors. *American journal of physiology Regulatory, integrative and comparative physiology* 291: R1825-1834, 2006.
11. **Burrell LM, Risvanis J, Dean RG, Patel SK, Velkoska E, and Johnston CI**. Age-dependent regulation of renal vasopressin V(1A) and V(2) receptors in rats with genetic hypertension: implications for the treatment of hypertension. *J Am Soc Hypertens* 7: 3-13, 2013.
12. **Campean V, Theilig F, Paliege A, Breyer M, and Bachmann S**. Key enzymes for renal prostaglandin synthesis: site-specific expression in rodent kidney (rat, mouse). *American journal of physiology Renal physiology* 285: F19-32, 2003.
13. **Capdevila J, and Wang W**. Role of cytochrome P450 epoxygenase in regulating renal membrane transport and hypertension. *Curr Opin Nephrol Hypertens* 22: 163-169, 2013.
14. **Crofton JT, Share L, Shade RE, Allen C, and Tarnowski D**. Vasopressin in the rat with spontaneous hypertension. *The American journal of physiology* 235: H361-366, 1978.
15. **Culpepper RM, and Andreoli TE**. Interactions among prostaglandin E2, antidiuretic hormone, and cyclic adenosine monophosphate in modulating Cl- absorption in single mouse medullary thick ascending limbs of Henle. *J Clin Invest* 71: 1588-1601, 1983.
16. **Dichlberger A, Schlager S, Kovanen PT, and Schneider WJ**. Lipid droplets in activated mast cells - a significant source of triglyceride-derived arachidonic acid for eicosanoid production. *European journal of pharmacology* 785: 59-69, 2016.
17. **Dietrich A, Mathia S, Kaminski H, Mutig K, Rosenberger C, Mrowka R, Bachmann S, and Paliege A**. Chronic activation of Vasopressin V2 receptor signaling lowers renal medullary oxygen levels in rats. *Acta physiologica* 2013.
18. **El-Sherbeni AA, Aboutabl ME, Zordoky BN, Anwar-Mohamed A, and El-Kadi AO**. Determination of the dominant arachidonic Acid cytochrome p450 monooxygenases in rat heart, lung, kidney, and liver: protein expression and metabolite kinetics. *AAPS J* 15: 112-122, 2013.
19. **Enayetallah AE, French RA, Thibodeau MS, and Grant DF**. Distribution of soluble epoxide hydrolase and of cytochrome P450 2C8, 2C9, and 2J2 in human tissues. *J Histochem Cytochem* 52: 447-454, 2004.
20. **Fromel T, Jungblut B, Hu J, Trouvain C, Barbosa-Sicard E, Popp R, Liebner S, Dimmeler S, Hammock BD, and Fleming I**. Soluble epoxide hydrolase regulates hematopoietic progenitor cell function via generation of fatty acid diols. *Proceedings of the National Academy of Sciences of the United States of America* 109: 9995-10000, 2012.
21. **Greger R**. Cation selectivity of the isolated perfused cortical thick ascending limb of Henle's loop of rabbit kidney. *Pflugers Archiv : European journal of physiology* 390: 30-37, 1981.
22. **Greger R, Oberleithner H, Schlatter E, Cassola AC, and Weidtke C**. Chloride activity in cells of isolated perfused cortical thick ascending limbs of rabbit kidney. *Pflugers Archiv : European journal of physiology* 399: 29-34, 1983.

23. **Grider JS, Falcone JC, Kilpatrick EL, Ott CE, and Jackson BA**. P450 arachidonate metabolites mediate bradykinin-dependent inhibition of NaCl transport in the rat thick ascending limb. *Can J Physiol Pharmacol* 75: 91-96, 1997.
24. **Harris RC, Jr.** Cyclooxygenase-2 inhibition and renal physiology. *The American journal of cardiology* 89: 10D-17D, 2002.
25. **Harris TR, and Hammock BD**. Soluble epoxide hydrolase: gene structure, expression and deletion. *Gene* 526: 61-74, 2013.
26. **He H, Podymow T, Zimpelmann J, and Burns KD**. NO inhibits Na+-K+-2Cl- cotransport via a cytochrome P-450-dependent pathway in renal epithelial cells (MMDD1). *American journal of physiology Renal physiology* 284: F1235-1244, 2003.
27. **Hennebold JD, Mah K, Perez W, Vance JE, Stouffer RL, Morisseau C, Hammock BD, and Adashi EY**. Identification and characterization of an ovary-selective isoform of epoxide hydrolase. *Biol Reprod* 72: 968-975, 2005.
28. **Hercule HC, Schunck WH, Gross V, Seringer J, Leung FP, Weldon SM, da Costa Goncalves A, Huang Y, Luft FC, and Gollasch M**. Interaction between P450 eicosanoids and nitric oxide in the control of arterial tone in mice. *Arterioscler Thromb Vasc Biol* 29: 54-60, 2009.
29. **Houillier P, Chambrey R, Achard JM, Froissart M, Poggioli J, and Paillard M**. Signaling pathways in the biphasic effect of angiotensin II on apical Na/H antiport activity in proximal tubule. *Kidney international* 50: 1496-1505, 1996.
30. **Imig JD**. Epoxides and soluble epoxide hydrolase in cardiovascular physiology. *Physiol Rev* 92: 101-130, 2012.
31. **Imig JD, Navar LG, Roman RJ, Reddy KK, and Falck JR**. Actions of epoxygenase metabolites on the preglomerular vasculature. *Journal of the American Society of Nephrology : JASN* 7: 2364-2370, 1996.
32. **Imig JD, Zhao X, Capdevila JH, Morisseau C, and Hammock BD**. Soluble epoxide hydrolase inhibition lowers arterial blood pressure in angiotensin II hypertension. *Hypertension (Dallas, Tex : 1979)* 39: 690-694, 2002.
33. **Jung O, Brandes RP, Kim IH, Schweda F, Schmidt R, Hammock BD, Busse R, and Fleming I**. Soluble epoxide hydrolase is a main effector of angiotensin II-induced hypertension. *Hypertension (Dallas, Tex : 1979)* 45: 759-765, 2005.
34. **Kaergel E, Muller DN, Honeck H, Theuer J, Shagdarsuren E, Mullally A, Luft FC, and Schunck WH**. P450-dependent arachidonic acid metabolism and angiotensin II-induced renal damage. *Hypertension (Dallas, Tex : 1979)* 40: 273-279, 2002.
35. **Kato Y, Fuchi N, Saburi H, Nishimura Y, Watanabe A, Yagi M, Nakadera Y, Higashi E, Yamada M, and Aoki T**. Discovery of 2,8-diazaspiro[4.5]decane-based trisubstituted urea derivatives as highly potent soluble epoxide hydrolase inhibitors and orally active drug candidates for treating hypertension. *Bioorg Med Chem Lett* 23: 5975-5979, 2013.
36. **Kawaguchi H, Okamoto H, Saito H, and Yasuda H**. Renal phospholipase C and diglyceride lipase activity in spontaneously hypertensive rats. *Hypertension (Dallas, Tex : 1979)* 10: 100-106, 1987.
37. **Knepper MA, Kwon TH, and Nielsen S**. Molecular physiology of water balance. *N Engl J Med* 372: 1349-1358, 2015.
38. **Lee JP, Yang SH, Lee HY, Kim B, Cho JY, Paik JH, Oh YJ, Kim DK, Lim CS, and Kim YS**. Soluble epoxide hydrolase activity determines the severity of ischemia-reperfusion injury in kidney. *PLoS One* 7: e37075, 2012.
39. **Li Y, Yamada H, Kita Y, Suzuki M, Endo Y, Horita S, Yamazaki O, Shimizu T, Seki G, and Fujita T**. Arachidonic acid metabolites inhibit the stimulatory effect of angiotensin II in renal proximal tubules. *Hypertension research : official journal of the Japanese Society of Hypertension* 31: 2155-2164, 2008.
40. **Livak KJ, and Schmittgen TD**. Analysis of relative gene expression data using real-time quantitative PCR and the 2(-Delta Delta C(T)) Method. *Methods* 25: 402-408, 2001.
41. **Luria A, Weldon SM, Kabcenell AK, Ingraham RH, Matera D, Jiang H, Gill R, Morisseau C, Newman JW, and Hammock BD**. Compensatory mechanism for homeostatic blood pressure regulation in Ephx2 gene-disrupted mice. *The Journal of biological chemistry* 282: 2891-2898, 2007.
42. **Madhun ZT, Goldthwait DA, McKay D, Hopfer U, and Douglas JG**. An epoxygenase metabolite of arachidonic acid mediates angiotensin II-induced rises in cytosolic calcium in rabbit proximal tubule epithelial cells. *The Journal of clinical investigation* 88: 456-461, 1991.

43. **Marova EI, Goncharov NP, Kolesnikova GS, Arapova SD, and Lapshina AM**. The response of corticotropin and adrenal steroids to desmopressin stimulation in patients with various forms of hypercortisolism. *Hormones (Athens, Greece)* 7: 243-250, 2008.
44. **Monti J, Fischer J, Paskas S, Heinig M, Schulz H, Gosele C, Heuser A, Fischer R, Schmidt C, Schirdewan A, Gross V, Hummel O, Maatz H, Patone G, Saar K, Vingron M, Weldon SM, Lindpaintner K, Hammock BD, Rohde K, Dietz R, Cook SA, Schunck WH, Luft FC, and Hubner N**. Soluble epoxide hydrolase is a susceptibility factor for heart failure in a rat model of human disease. *Nat Genet* 40: 529-537, 2008.
45. **Moss NG, Kopple TE, and Arendshorst WJ**. Renal vasoconstriction by vasopressin V1a receptors is modulated by nitric oxide, prostanoids, and superoxide but not the ADP ribosyl cyclase CD38. *American journal of physiology Renal physiology* 306: F1143-1154, 2014.
46. **Mutig K, Paliege A, Kahl T, Jons T, Muller-Esterl W, and Bachmann S**. Vasopressin V2 receptor expression along rat, mouse, and human renal epithelia with focus on TAL. *American journal of physiology Renal physiology* 293: F1166-1177, 2007.
47. **Nofziger C, Brown KK, Smith CD, Harrington W, Murray D, Bisi J, Ashton TT, Maurio FP, Kalsi K, West TA, Baines D, and Blazer-Yost BL**. PPARgamma agonists inhibit vasopressin-mediated anion transport in the MDCK-C7 cell line. *American journal of physiology Renal physiology* 297: F55-62, 2009.
48. **Oguro A, Fujita N, and Imaoka S**. Regulation of soluble epoxide hydrolase (sEH) in mice with diabetes: high glucose suppresses sEH expression. *Drug metabolism and pharmacokinetics* 24: 438-445, 2009.
49. **Okada H, Suzuki H, Kanno Y, and Saruta T**. Effect of nonpeptide vasopressin receptor antagonists on developing, and established DOCA-salt hypertension in rats. *Clin Exp Hypertens* 17: 469-483, 1995.
50. **Ostrowski NL, Young WS, 3rd, Knepper MA, and Lolait SJ**. Expression of vasopressin V1a and V2 receptor messenger ribonucleic acid in the liver and kidney of embryonic, developing, and adult rats. *Endocrinology* 133: 1849-1859, 1993.
51. **Paliege A, Roeschel T, Neymeyer H, Seidel S, Kahl T, Daigeler AL, Mutig K, Mrowka R, Ferreri NR, Wilson BS, Himmerkus N, Bleich M, and Bachmann S**. Group VIA phospholipase A2 is a target for vasopressin signaling in the thick ascending limb. *American journal of physiology Renal physiology* 302: F865-874, 2012.
52. **Paliege A, Rosenberger C, Bondke A, Sciesielski L, Shina A, Heyman SN, Flippin LA, Arend M, Klaus SJ, and Bachmann S**. Hypoxia-inducible factor-2alpha-expressing interstitial fibroblasts are the only renal cells that express erythropoietin under hypoxia-inducible factor stabilization. *Kidney international* 77: 312-318, 2010.
53. **Pan YJ, Tao ZF, Wang Q, Lu M, Guan YF, Zhu Y, and Wang Y**. [Expression and role of soluble epoxide hydrolase in renal tissue of two kidneys one clip hypertension rats model]. *Beijing da xue xue bao Yi xue ban = Journal of Peking University Health sciences* 43: 820-826, 2011.
54. **Pietranera L, Saravia FE, McEwen BS, Lucas LL, Johnson AK, and De Nicola AF**. Changes in Fos expression in various brain regions during deoxycorticosterone acetate treatment: relation to salt appetite, vasopressin mRNA and the mineralocorticoid receptor. *Neuroendocrinology* 74: 396-406, 2001.
55. **Pinot F, Grant DF, Spearow JL, Parker AG, and Hammock BD**. Differential regulation of soluble epoxide hydrolase by clofibrate and sexual hormones in the liver and kidneys of mice. *Biochemical pharmacology* 50: 501-508, 1995.
56. **Rieg T, Tang T, Murray F, Schroth J, Insel PA, Fenton RA, Hammond HK, and Vallon V**. Adenylate cyclase 6 determines cAMP formation and aquaporin-2 phosphorylation and trafficking in inner medulla. *Journal of the American Society of Nephrology : JASN* 21: 2059-2068, 2010.
57. **Roman RJ**. P-450 metabolites of arachidonic acid in the control of cardiovascular function. *Physiol Rev* 82: 131-185, 2002.
58. **Roman RJ, Maier KG, Sun CW, Harder DR, and Alonso-Galicia M**. Renal and cardiovascular actions of 20-hydroxyeicosatetraenoic acid and epoxyeicosatrienoic acids. *Clin Exp Pharmacol Physiol* 27: 855-865, 2000.
59. **Sarkis A, Ito O, Mori T, Kohzuki M, Ito S, Verbalis J, Cowley AW, Jr., and Roman RJ**. Cytochrome P-450-dependent metabolism of arachidonic acid in the kidney of rats with diabetes insipidus. *American journal of physiology Renal physiology* 289: F1333-1340, 2005.

60. **Sarmiento JM, Ehrenfeld P, Anazco CC, Reyes CE, Troncoso S, Figueroa CD, Muller-Esterl W, and Gonzalez CB**. Differential distribution of the vasopressin V receptor along the rat nephron during renal ontogeny and maturation. *Kidney international* 68: 487-496, 2005.
61. **Schmelzer KR, Kubala L, Newman JW, Kim IH, Eiserich JP, and Hammock BD**. Soluble epoxide hydrolase is a therapeutic target for acute inflammation. *Proceedings of the National Academy of Sciences of the United States of America* 102: 9772-9777, 2005.
62. **Sinal CJ, Miyata M, Tohkin M, Nagata K, Bend JR, and Gonzalez FJ**. Targeted disruption of soluble epoxide hydrolase reveals a role in blood pressure regulation. *The Journal of biological chemistry* 275: 40504-40510, 2000.
63. **Sladek CD, Blair ML, Sterling C, and Mangiapane ML**. Attenuation of spontaneous hypertension in rats by a vasopressin antagonist. *Hypertension (Dallas, Tex : 1979)* 12: 506-512, 1988.
64. **Staudinger R, Escalante B, Schwartzman ML, and Abraham NG**. Effects of epoxyeicosatrienoic acids on 86Rb uptake in renal epithelial cells. *Journal of cellular physiology* 160: 69-74, 1994.
65. **Sun P, Lin DH, Wang T, Babilonia E, Wang Z, Jin Y, Kemp R, Nasjletti A, and Wang WH**. Low Na intake suppresses expression of CYP2C23 and arachidonic acid-induced inhibition of ENaC. *American journal of physiology Renal physiology* 291: F1192-1200, 2006.
66. **Tahara A, Tsukada J, Tomura Y, Wada K, Kusayama T, Ishii N, Yatsu T, Uchida W, Taniguchi N, and Tanaka A**. Alterations of renal vasopressin V1A and V2 receptors in spontaneously hypertensive rats. *Pharmacology* 67: 106-112, 2003.
67. **Turner MR, and Pallone TL**. Vasopressin constricts outer medullary descending vasa recta isolated from rat kidneys. *The American journal of physiology* 272: F147-151, 1997.
68. **Ulu A, Davis BB, Tsai HJ, Kim IH, Morisseau C, Inceoglu B, Fiehn O, Hammock BD, and Weiss RH**. Soluble epoxide hydrolase inhibitors reduce the development of atherosclerosis in apolipoprotein e-knockout mouse model. *J Cardiovasc Pharmacol* 52: 314-323, 2008.
69. **Walkowska A, Skaroupkova P, Huskova Z, Vanourkova Z, Chabova VC, Tesar V, Kramer HJ, Falck JR, Imig JD, Kompanowska-Jezierska E, Sadowski J, and Cervenka L**. Intrarenal cytochrome P-450 metabolites of arachidonic acid in the regulation of the nonclipped kidney function in two-kidney, one-clip Goldblatt hypertensive rats. *Journal of hypertension* 28: 582-593, 2010.
70. **Weichert W, Paliege A, Provoost AP, and Bachmann S**. Upregulation of juxtaglomerular NOS1 and COX-2 precedes glomerulosclerosis in fawn-hooded hypertensive rats. *American journal of physiology Renal physiology* 280: F706-714, 2001.
71. **Welker P, Bohlick A, Mutig K, Salanova M, Kahl T, Schluter H, Blottner D, Ponce-Coria J, Gamba G, and Bachmann S**. Renal Na+-K+-Cl- cotransporter activity and vasopressin-induced trafficking are lipid raft-dependent. *American journal of physiology Renal physiology* 295: F789-802, 2008.
72. **Williams TD, Lightman SL, and Leadbeater MJ**. Hormonal and cardiovascular responses to DDAVP in man. *Clinical endocrinology* 24: 89-96, 1986.
73. **Yang T, Schnermann JB, and Briggs JP**. Regulation of cyclooxygenase-2 expression in renal medulla by tonicity in vivo and in vitro. *The American journal of physiology* 277: F1-9, 1999.
74. **Yoshida M, Ueda S, Soejima H, Tsuruta K, and Ikegami K**. Effects of prostaglandin E2 and I2 on renal cortical and medullary blood flow in rabbits. *Arch Int Pharmacodyn Ther* 282: 108-117, 1986.
75. **Yu Z, Davis BB, Morisseau C, Hammock BD, Olson JL, Kroetz DL, and Weiss RH**. Vascular localization of soluble epoxide hydrolase in the human kidney. *American journal of physiology Renal physiology* 286: F720-726, 2004.
76. **Yu Z, Huse LM, Adler P, Graham L, Ma J, Zeldin DC, and Kroetz DL**. Increased CYP2J expression and epoxyeicosatrienoic acid formation in spontaneously hypertensive rat kidney. *Mol Pharmacol* 57: 1011-1020, 2000.
77. **Zhang MZ, Sanchez Lopez P, McKanna JA, and Harris RC**. Regulation of cyclooxygenase expression by vasopressin in rat renal medulla. *Endocrinology* 145: 1402-1409, 2004.
78. **Zhao X, Yamamoto T, Newman JW, Kim IH, Watanabe T, Hammock BD, Stewart J, Pollock JS, Pollock DM, and Imig JD**. Soluble epoxide hydrolase inhibition protects the kidney from hypertension-induced damage. *Journal of the American Society of Nephrology : JASN* 15: 1244-1253, 2004.

Table 1

Gene Title	Gene Symbol	mRNA Accession	Probe Set ID	x-fold of control	p
epoxide hydrolase 2, cytoplasmic	EPHX2	NM_022936	Rn.54495_at	2.45	0.04*
cytochrome P450, family 2, subfamily c, polypeptide 11	Cyp2c11	NM_019184	1387328_at	1.3	0.68
cytochrome P450, family 2, subfamily c, polypeptide 23	Cyp2c23	NM_031839	1367988_at	0.97	0.52
cytochrome P450, family 2, subfamily j, polypeptide 3	Cyp2j3	NM_175766	1370706_a_at	0.99	0.8
cytochrome P450, family 2, subfamily j, polypeptide 4	Cyp2j4	NM_023025	Rn.44992_at	0.78	0.003*
cytochrome P450, family 2, subfamily j, polypeptide 10	Cyp2j10	NM_001134980	Rn.34638_at	0.95	0.26

Figure 1

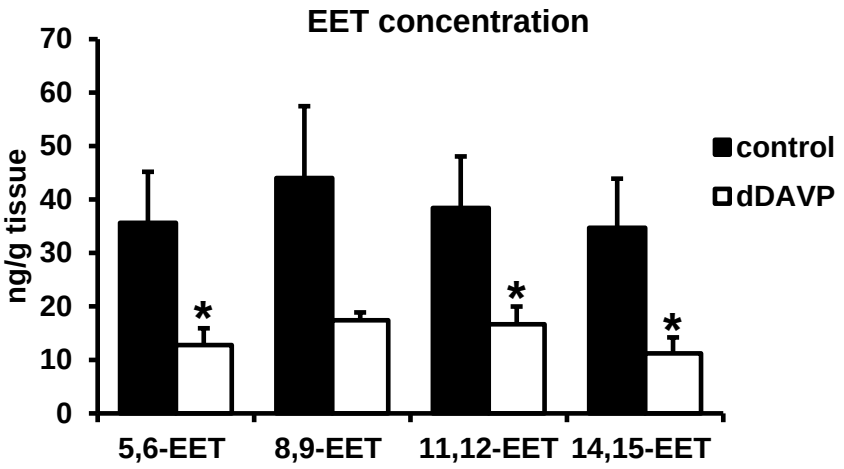
EET concentration
ng/g tissue
70
60
50
40
30
20
10
0
control
dDAVP
*
*
*
5,6-EET
8,9-EET
11,12-EET
14,15-EET

Figure 2

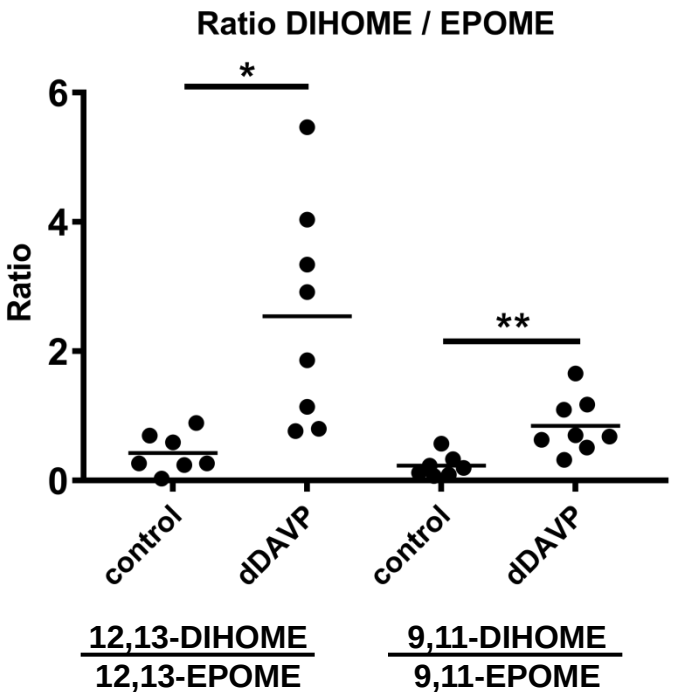
Ratio DIHOME / EPOME
*
**
6
4
2
0
Ratio
control
dDAVP
control
dDAVP
12,13-DIHOME
12,13-EPOME
9,11-DIHOME
9,11-EPOME

Figure 3

A

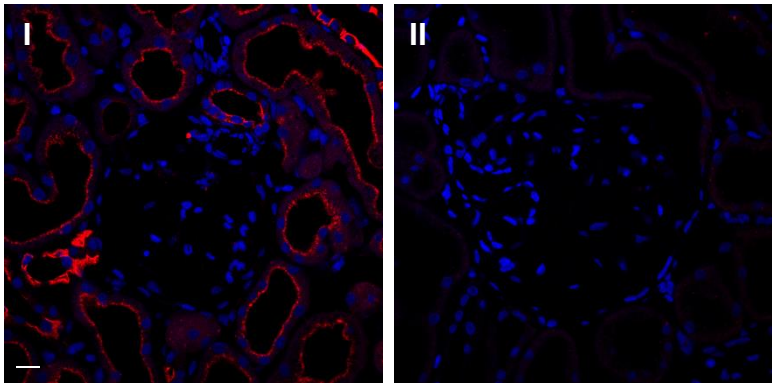

control blockade

B

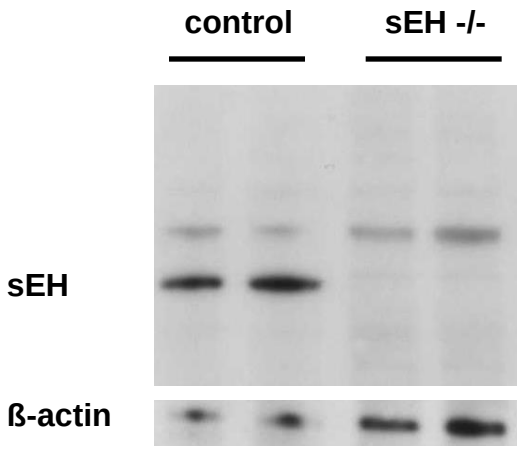

C

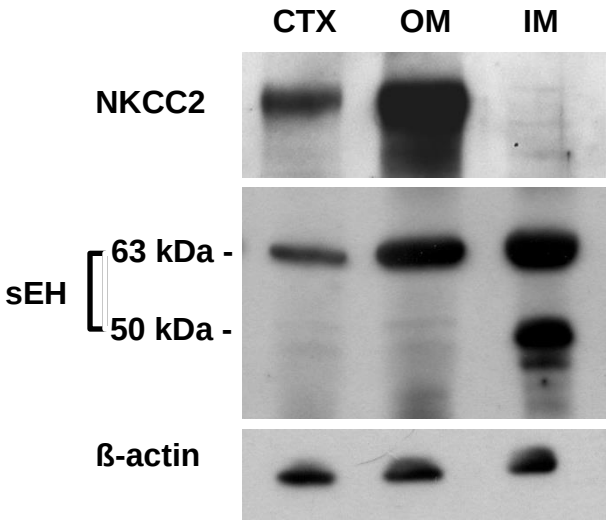

Figure 4

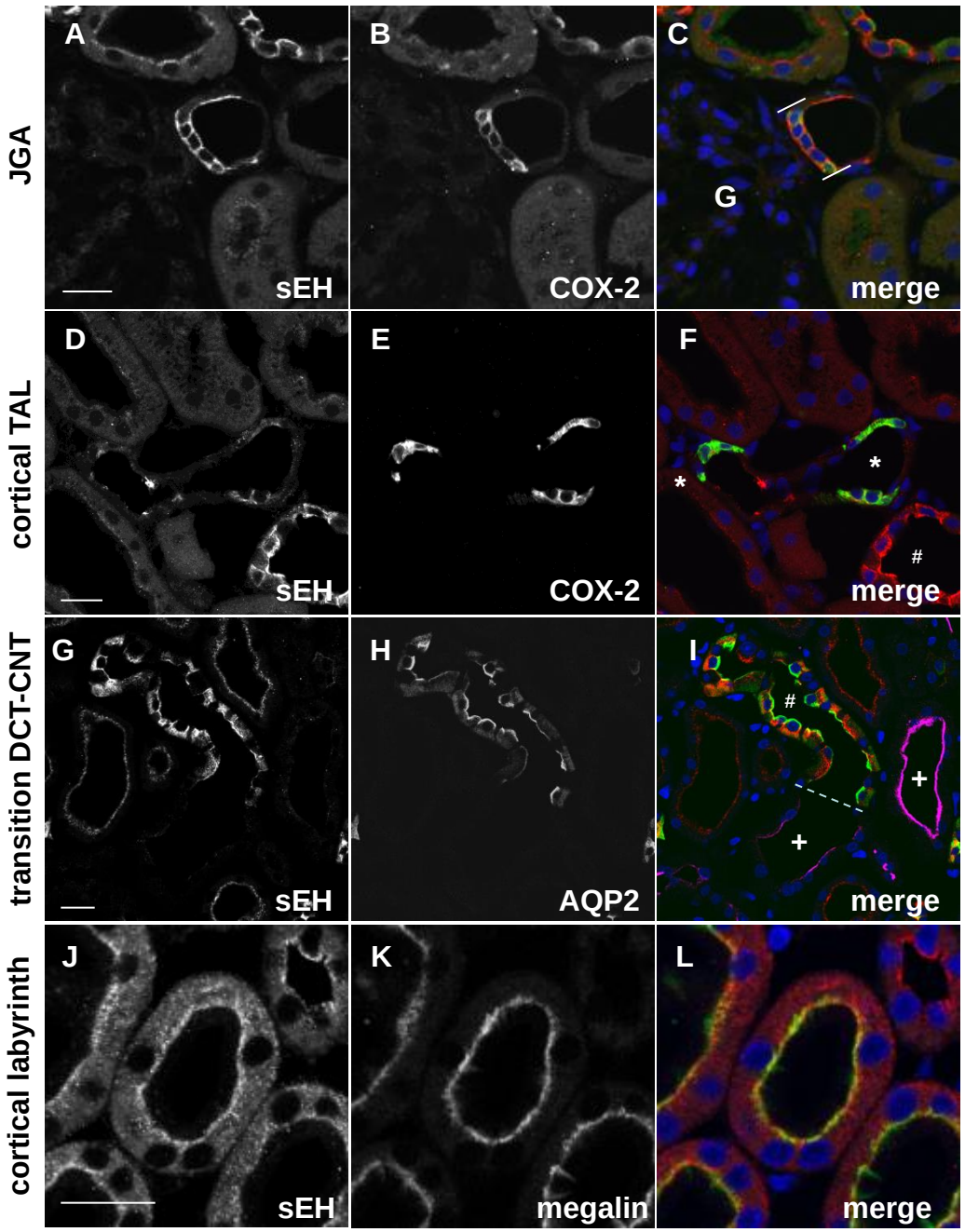
JGA
cortical TAL
transition DCT-CNT
cortical labyrinth
A
sEH
B
COX-2
C
G
merge
D
sEH
E
COX-2
F
*
*
#
merge
G
sEH
H
AQP2
I
#
+
+
merge
J
sEH
K
megalin
L
merge

Figure 5

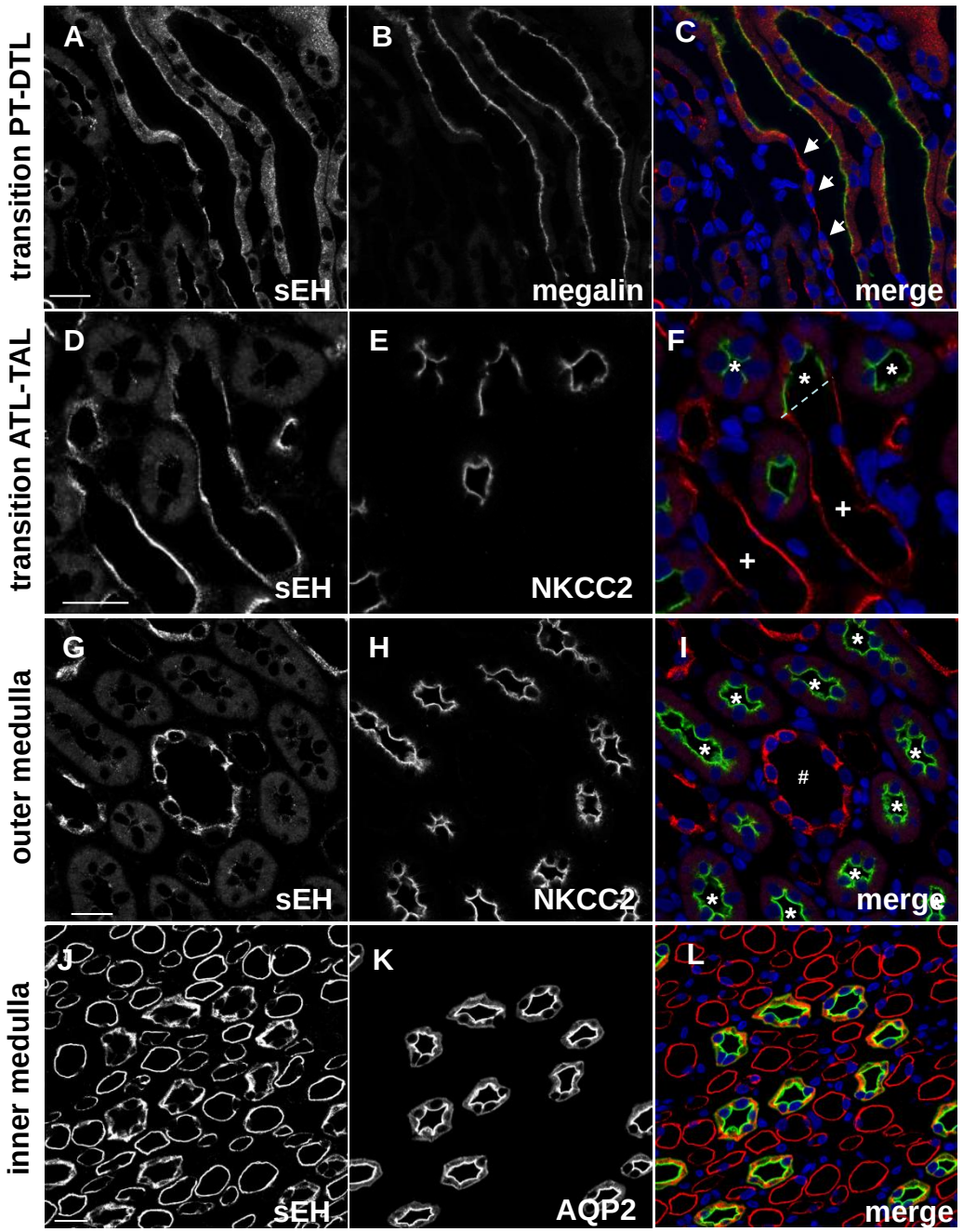
transition PT-DTL
transition ATL-TAL
outer medulla
inner medulla
A
sEH
B
megalin
C
merge
D
sEH
E
NKCC2
F
merge
G
sEH
H
NKCC2
I
merge
J
sEH
K
AQP2
L
merge

Figure 6

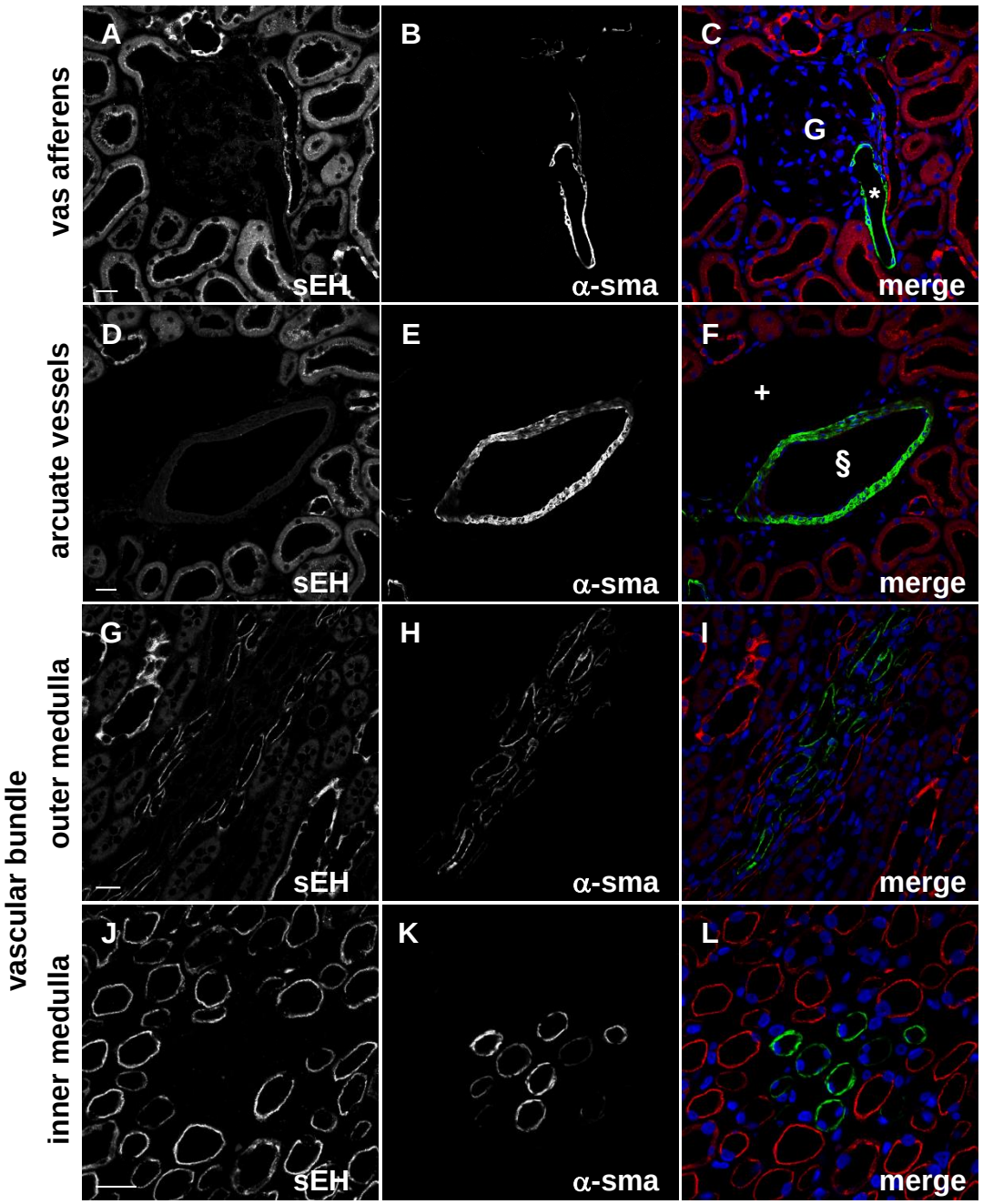
vas afferens
arcuate vessels
vascular bundle
outer medulla
inner medulla
A
B
C
G
*
sEH
α-sma
merge
D
E
F
+
§
sEH
α-sma
merge
G
H
I
sEH
α-sma
merge
J
K
L
sEH
α-sma
merge

Figure 7

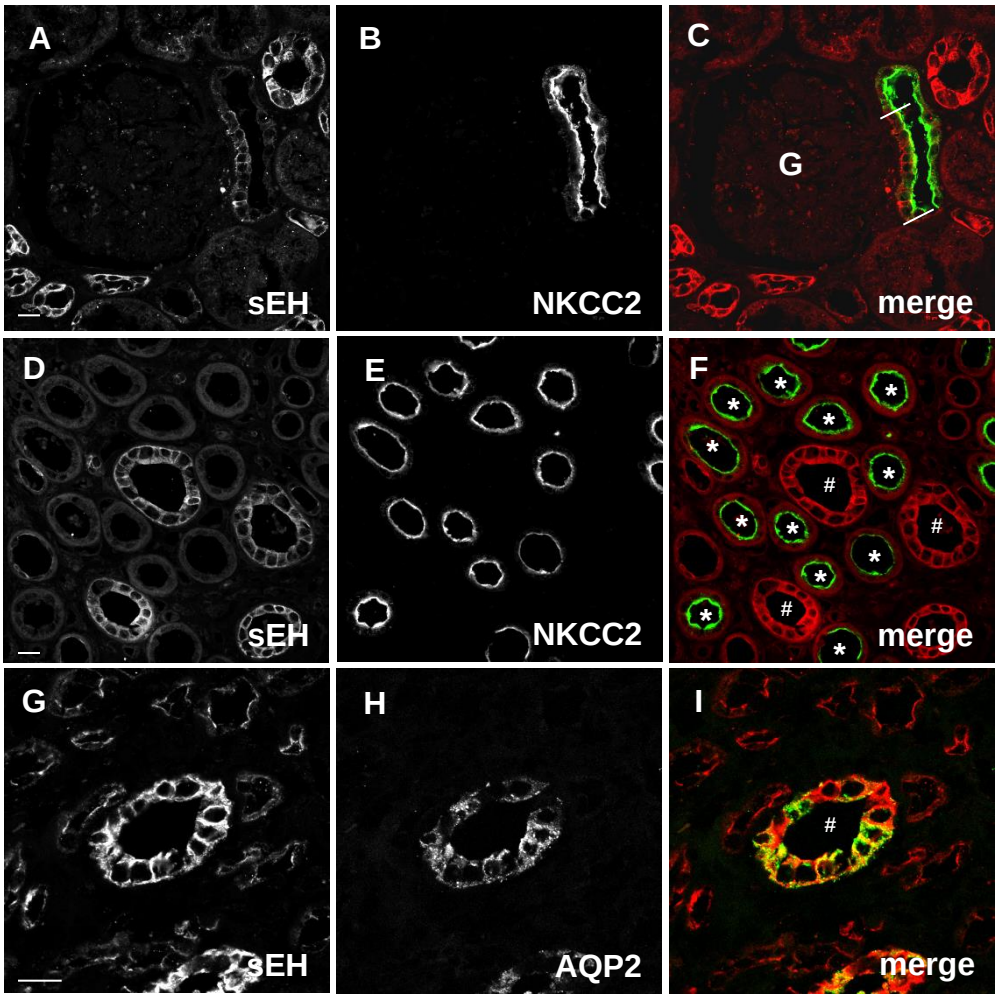

Figure 8

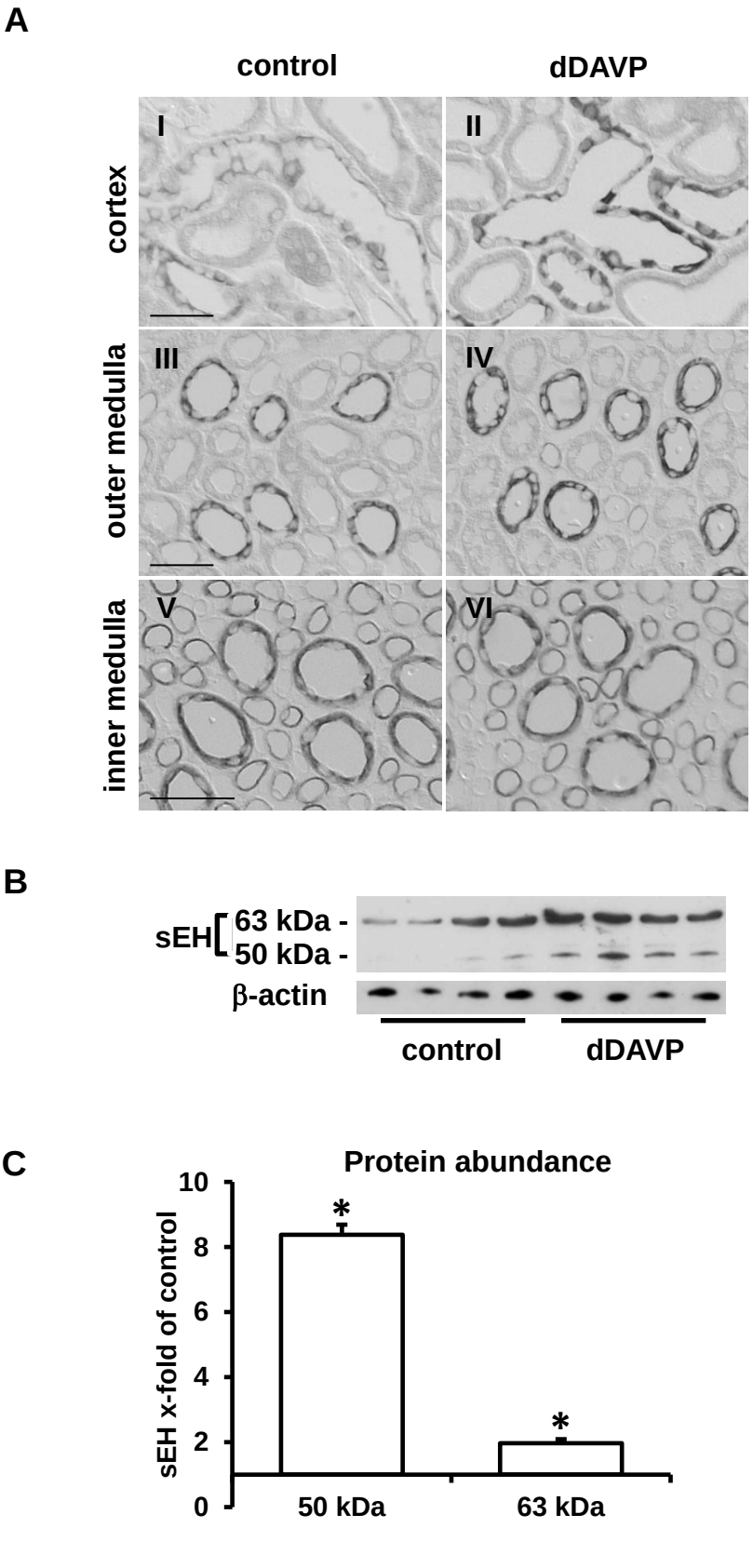
A
control
dDAVP
cortex
outer medulla
inner medulla
I
II
III
IV
V
VI
B
sEH
63 kDa -
50 kDa -
β-actin
control
dDAVP
C
Protein abundance
sEH x-fold of control
10
8
6
4
2
0
*
*
50 kDa
63 kDa

Figure 9

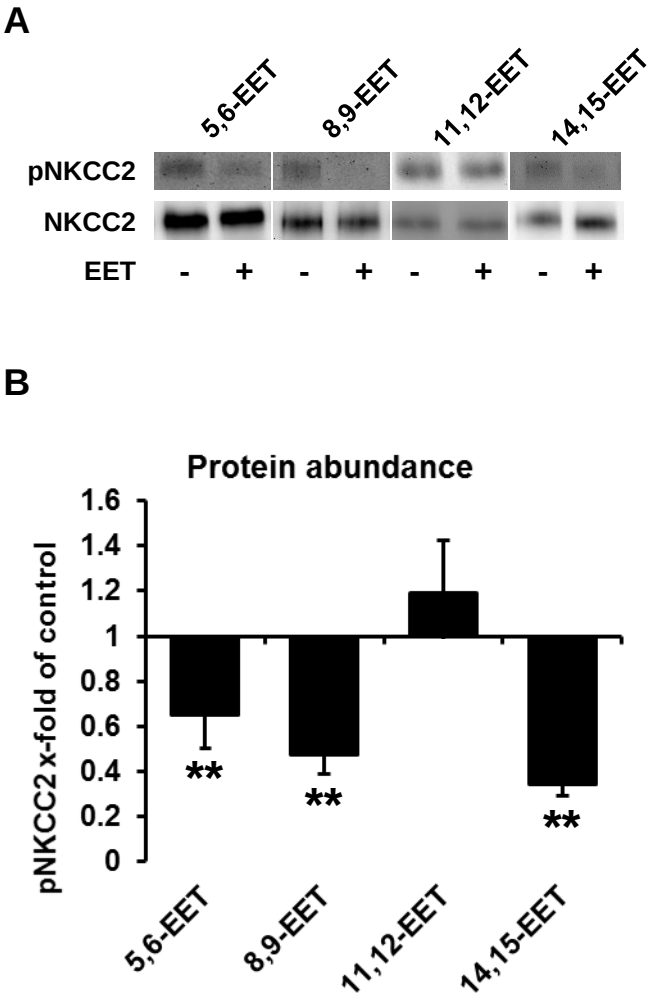
A
5,6-EET
8,9-EET
11,12-EET
14,15-EET
pNKCC2
NKCC2
EET - + - + - + - +
B
Protein abundance
pNKCC2 x-fold of control
1.6
1.4
1.2
1
0.8
0.6
0.4
0.2
0
**
**
**
5,6-EET
8,9-EET
11,12-EET
14,15-EET

Figure 10

A

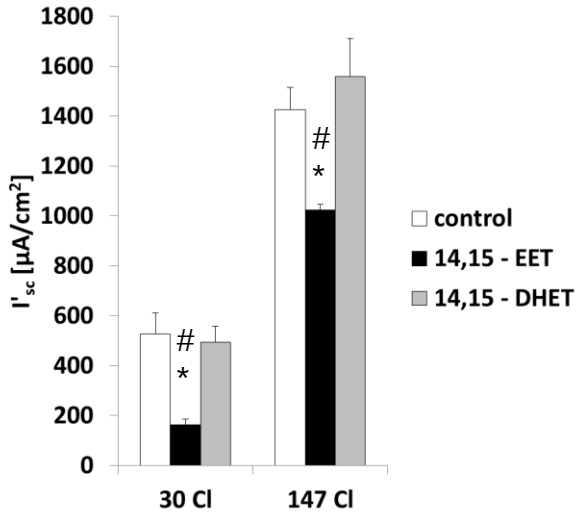

B

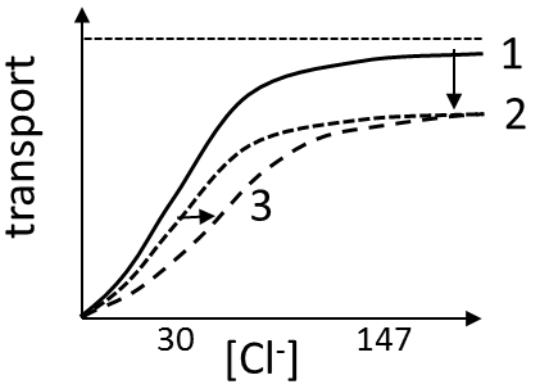

C

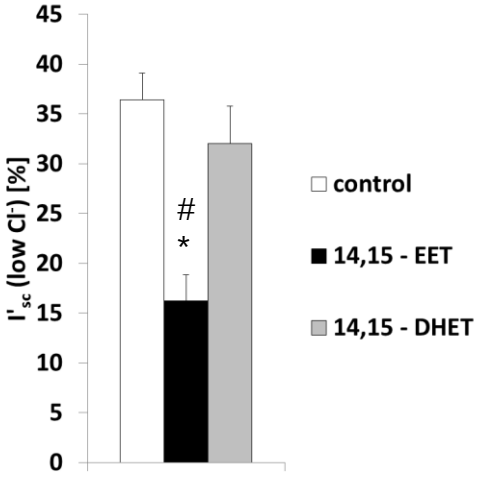

D

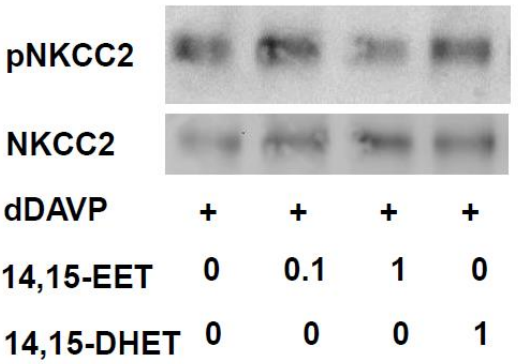

Figure 11